THE JOURNAL OF PHYSICAL CHEMISTRY LETTERS
A JOURNAL OF THE AMERICAN CHEMICAL SOCIETY

pubs.acs.org/JPCL

Letter

Plasmonic Enhancement and Angular Control of Narrow-Emitting Europium-Based Luminescence

Aleksandr Yu. Frolov, Arseny Yu. Gladkikh, Matvey P. Belov, Vladimir V. Popov, Valentina V. Utochnikova,* and Andrey A. Fedyanin*

Cite This: J. Phys. Chem. Lett. 2025, 16, 11590−11596

Read Online

ACCESS | Metrics & More | Article Recommendations | Supporting Information

ABSTRACT: Eu-based emitters are known to offer narrow-band red luminescence, making them ideal for use as OLEDs. However, their long excited-state lifetime limits device efficiency compared to other materials. This paper aims to demonstrate that the integrating plasmonic resonances can reduce the lifetime and enable the directional emission outcoupling of various kinds of luminescent materials. Here, we employ one-dimensional aluminum plasmonic crystals (PCs) to control the directionality of photoluminescence in $Eu(dbm)_3(TDZP)$ (dbm = dibenzoylmethanate, TDZP = thiadiazolophenanthroline). The PCs with tailored periodicity were fabricated to achieve spectral overlap between surface plasmon resonances and the electric dipole transition of europium at 612 nm. Tuning periodicity directed the emission to near ±7° with a narrow angular divergence of 5°. At the resonance, the 4-fold enhancement in photoluminescence intensity was observed. Coupling the emission with surface plasmons and outcoupling it to the far-field decreased the lifetime of $Eu(dbm)_3(TDZP)$ by 1.7 times. This study therefore demonstrates the potential of plasmonic engineering to overcome the limitations of lanthanide emitters.

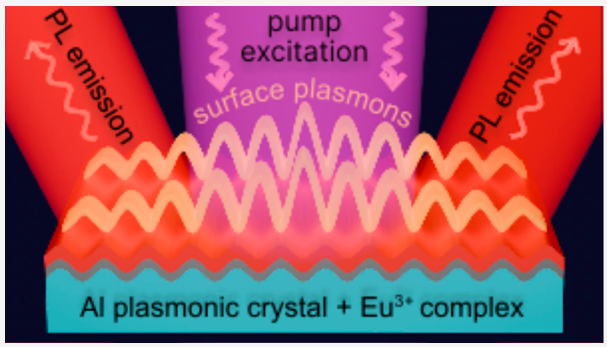

Organic light-emitting diodes (OLEDs) have become an essential technology in modern optoelectronics due to their efficiency, flexibility, and potential for low-cost fabrication.[1] However, despite significant advances, several challenges still need to be addressed to further optimize their performance. One of OLEDs' major limitations is their relatively low light outcoupling efficiency, which typically does not exceed 20%.[2] It stems from the waveguiding effects, whereby light emitted at angles far from the surface normally becomes trapped within the device layers. Another critical issue is the necessity for narrow emission bands, especially when it comes to OLED applications in high-resolution displays and advanced lighting technologies.[3,4] Such narrow emission bands are a unique feature of lanthanide-based emitters, attributed to the intraconfigurational 4f−4f electronic transitions.[5,6] These transitions, shielded from the ligand environment, result in exceptionally sharp spectral lines that are highly desirable for the color purity. Meanwhile, the same electronic structure that ensures narrow emission bands also leads to a long photoluminescence lifetime, posing significant challenges for the performance of OLEDs based on lanthanide complexes.[7] Thus, enhancing the efficiency of lanthanide-based OLEDs remains a key objective in photonics research.

One promising approach to solving these issues is the integrating plasmonic[8−15] and all-dielectric[16−21] nanostructures in order to manipulate light emission properties. This mechanism is based on the excitation of surface plasmons (SPs) and Mie resonances in individual optical resonators that enhance the excitation efficiency as well as radiative decay rates and influence the directionality of emission with the modification of extraction efficiency. An arrangement of subwavelength resonators in one- or two-dimensional arrays, called metasurfaces,[22] allows for additional and precise control of luminescent intensity and directivity. Various types of plasmonic[23−29] and all-dielectric[30−35] metasurfaces boost the photoluminescent signal of quantum dots, fluorescent molecules, and other emitters. Regarding the lanthanide complexes, previous studies have focused on enhancing photoluminescence and improving its directivity with high-index nanoparticles[36] and metasurfaces,[35,37] or, plasmonic nanoparticles[8,9,14,15] and metasurfaces,[23] as well as realizing upconverting lasing.[38−40]

Despite the low losses of all-dielectric metasurfaces, the plasmonic ones exhibit a strongly enhanced electric field localization near the surface and can be implemented as electrodes in the electroluminescent OLED cells[41−44] that

Received: July 3, 2025
Revised: September 23, 2025
Accepted: September 23, 2025

https://doi.org/10.1021/acs.jpclett.5c02045
J. Phys. Chem. Lett. 2025, 16, 11590−11596

significantly expand their functionality. The first works on the combination of lanthanide complexes with plasmonic structures[8−10,14,15,23] have been devoted to the enhancement of photoluminescence intensity without the controlling its directivity. However, engineering the latter parameter to be angularly directed closer to the surface normal makes it possible to mitigate the waveguide losses present in actual OLED cells. Among the candidates to enhance the emission of lanthanide complexes and control its directivity are the surface plasmons excited in plasmonic crystals (PCs).[29,41,45−49] They present a periodically structured one- or two-dimensional metallic surface or arrays of plasmonic nanoparticles that support propagating surface plasmons or surface lattice modes, respectively. Their selective coupling with incident light and back reradiation to the far-field, governed by the surface plasmon dispersion law, opens up many possibilities for adjusting both the intensity and the angular directivity of the emission of lanthanide-based complexes.

In this work, we utilize aluminum plasmonic crystals, a one-dimensional periodically nanostructured aluminum surface, to enhance the photoluminescence and address the issue of light outcoupling efficiency in Eu-based OLEDs. The plasmonic resonances in aluminum-based nanostructures are only slightly affected by the presence of aluminum oxide,[50] which improves the stability of these devices. It was also chosen for its remarkable cost-effectiveness and high conductivity, which are important for OLED application and are therefore used in electroluminescent-based OLED cells.[51,52] The periodic structure of Al PCs is designed to selectively couple the photoluminescence of a Eu-based complex to propagating surface plasmon modes and decouple the emission toward a narrow angular range centered around the surface normal (0°) or other angles. Aligning the plasmonic modes of PCs with the emission wavelengths of europium complexes ensures that the luminescence is emitted preferentially in the direction that is optimal for extraction. By designing plasmonic crystals capable of redirecting emission predominantly along the surface normal (0°), we seek to overcome the waveguiding losses and improve the efficiency of lanthanide-based spectral OLEDs. This approach not only enhances the apparent brightness of lanthanide-based OLEDs but also addresses one of the key OLED limitations associated with their long lifetime that is reduced due to SPs.

In this study, we selected the europium complex, Eu(dbm)$_3$(TDZP) (dbm = dibenoylmethanate, TDZP = thiadiazolophenanthroline), as the emissive material.[53] This particular complex was chosen due to its well-known luminescence properties, including narrow-band emission and high photostability, which make it an ideal candidate for exploring directional light control in lanthanide-based systems. The europium complex Eu(dbm)$_3$(TDZP) was synthesized using the standard method[53] and characterized by a combination of several techniques (see Supporting Information (SI1)). Thin films were deposited via thermal vacuum evaporation, achieving a uniform layer thickness of 40 ± 5 nm, as confirmed by the atomic force microscopy (AFM) measurements shown in Figure S2 (SI1).

The one-dimensional PCs with tailored angular and spectral positions of SP resonances have been designed and fabricated to control the photoluminescence (PL) directivity and intensity of Eu-based complexes. The PCs under scrutiny represented aluminum periodic metal surfaces with various periodicities. They were fabricated using electron-beam lithography of the negative electronic resist which has been covered on the polymer substrate. After the development process and the formation of a periodic surface profile, the latter was covered by the Al film with a thickness of 35 nm. The periodicity and corrugation depth of the surface relief were adjusted by varying the electron beam exposure time. The surface profile of the fabricated PCs was characterized by using atomic force microscopy. Figures 1(a,b) shows the AFM maps

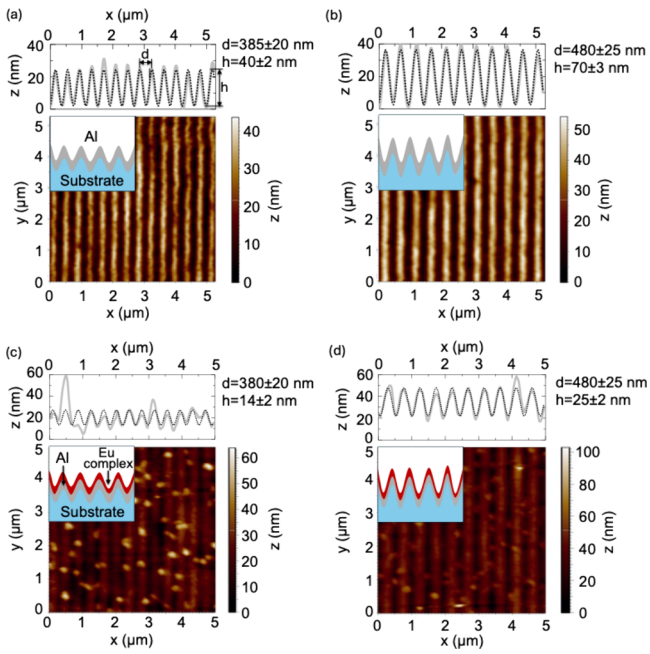

Figure 1. AFM images (bottom maps) and its cross sections (top graphs) of the fabricated one-dimensional Al plasmonic crystals with a period of d = 385 nm (a) and d = 480 nm (b). AFM images and its cross sections of the Al PCs with a period of d = 385 nm (c) and d = 480 nm (d) covered by a 40 nm film of the Eu(dbm)$_3$(TDZP) complex. The dotted curves on the graphs are the fits of AFM cross sections by $y(x) = A + 0.5h \times \sin(\frac{2\pi}{d}x + \varphi_0)$, where A, h, d, and φ_0 are adjustable parameters. The insets provide a schematic view of the fabricated samples.

of the two fabricated PCs and their cross sections along the x-direction (top graphs). The defined period (d) and the corrugation depth (h) of Al PCs were d = 385 ± 20 nm and h = 40 ± 2 nm for the first Al PC, and d = 480 ± 25 nm, h = 70 ± 3 nm for the second one. The angular-wavelength position and the spectral line shape of the SPs in the fabricated PCs were determined by measuring the angular dependence of the specularly reflected beam's reflectance spectra. The wavelength range spans from λ = 480 nm to λ = 800 nm and the angles of light incidence vary from 5° to 45°. More details on the experimental setup of angular-wavelength reflectance measurements can be found in the Supporting Information (SI2, Figure S3(a)). Figures 2(a,b) show the angular-wavelength reflectance maps of Al PCs with a period of 385 and 480 nm, respectively. Angular-dependent reflectance minima were observed in the reflectance spectra for both samples. They originated from the SPs excited by coupling with the diffraction orders of the grating. The angular-spectral position of the plasmon resonances in metallic gratings are defined by the following phase-matching condition:[54]

https://doi.org/10.1021/acs.jpclett.5c02045
J. Phys. Chem. Lett. 2025, 16, 11590−11596

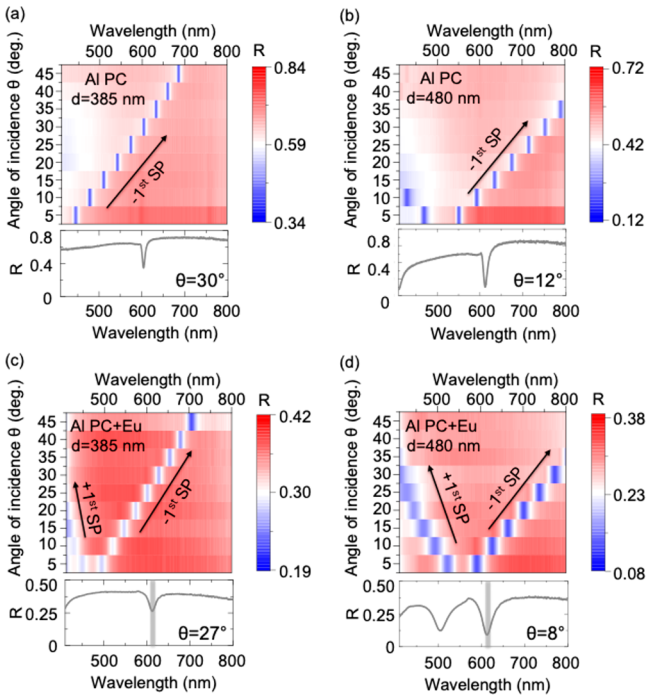

Figure 2. Maps show the angular-wavelength reflectance for aluminum plasmonic crystals without (a, b) and with (c, d) the Eu(dbm)$_3$(TDZP) complex film of 40 nm thickness. (a, c) Period of d = 385 nm and (b, d) period of d = 480 nm. The graphs below are the cross sections of R maps at angles θ, corresponding to the main electric dipole transition of the Eu^{3+} emission line (λ = 612 nm) marked by vertical gray stripes.

$$k_{spp} = Re\left\{\frac{\omega}{c}\sqrt{\frac{\varepsilon_m\varepsilon_d}{\varepsilon_m+\varepsilon_d}}\right\} = k_0 \sin\theta + mg \quad (1)$$

where ε_m and ε_d are the dielectric permittivity of metal and dielectric, ω and θ are the frequency and the incident angle of light, $k_0 = \omega/c$ is the wavevector of the incident light, $g = 2\pi/d$, d is the grating period, and $m = \pm1, \pm2$ is the number of the diffraction order. According to Equation 1 the reflectance minima observed at $\lambda > 400$ nm in the PC with d = 385 nm and at $\lambda > 500$ nm in the PC with d = 480 nm are associated with the excitation of the −1st order SP (m = −1). These minima are shifted to the reddish wavelength as the incident angle increases. In the case of the PC with d = 480 nm, the reflectance minima at $\lambda < 500$ nm are associated with the +1st order SP (m = +1). They are shifted to the blue spectral range as the incident angle increases. It should be noted that the reflectance spectral line width associated with SP excitation is dipper in the case of the PC with d = 480 nm (see the reflectance spectra below the maps in Figure 3(a), (b)). This is caused by a larger corrugation depth (70 nm) that provides a higher coupling efficiency of the incident light with surface plasmon.[55−57]

After the surface profile was characterized and measurements of the reflectance spectra were taken, thin films of the Eu(dbm)$_3$(TDZP) complex with a thickness of (40 ± 5) nm were deposited onto PCs via thermal vacuum evaporation. The AFM images of PCs with the Eu(dbm)$_3$(TDZP) complex are presented in Figure 1(c) (d = 385 nm) and Figure 1 (d) (d = 480 nm). The periodicity remains the same, whereas the corrugation depth decreases due to deposition of the film. The measured angular-wavelength reflectance maps are shown in

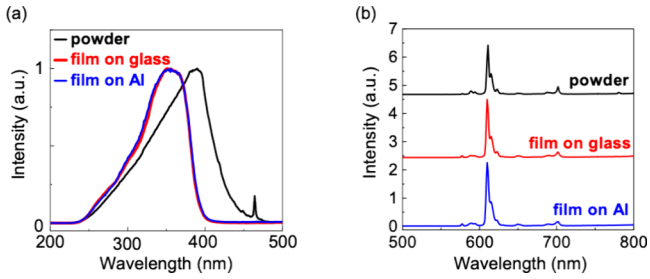

Figure 3. (a) Excitation and (b) emission spectra of the Eu(dbm)$_3$(TDZP) complex in powder (black curve) and thin-film states upon glass (red curve) and Al (blue curve) film. The excitation and emission spectra were normalized. The emission spectra are depicted with constant y-shift.

Figures 2(c,d) for the PCs + Eu(dbm)$_3$(TDZP) with d = 385 nm and d = 480 nm, respectively. The deposited Eu(dbm)$_3$(TDZP) film represents a dielectric layer with a refractive index of approximately 1.5 on the aluminum PC surface. Therefore, according to Equation 1, SP resonances of all orders are shifted to the long wavelength range. The resonances of the angular reflectance spectra were shifted to a reddish wavelength upon the Eu(dbm)$_3$(TDZP) complex deposition in comparison with the uncovered PCs. As a result, the resonance near the europium emission wavelength of 612 nm (the gray vertical stripe in Figures 2(c,d)) was observed at an incidence angle of approximately 27° and 8° for the PCs with d = 385 nm and d = 480 nm, respectively.

The photophysical properties of the europium complex were studied in both powder and thin-film states. Thin films were deposited on a quartz glass surface, an Al flat surface, and PC surfaces. The excitation spectra (Figure 3(a)) of film states (blue and red curves) exhibited a notable blue shift compared to the powder spectrum (black curve), indicating changes in the local environment and ligand field symmetry around Eu^{3+} ions upon film formation. However, the emission spectra (Figure 3(b)) in both powder and films were nearly identical and exhibited a dominant peak at 612 nm, characteristic of the hypersensitive $^5D_0 \rightarrow {}^7F_2$ electric dipole transition of the Eu^{3+} ion.

The photoluminescence angular intensity distributions of the europium complex films deposited on both PCs (d = 385 and d = 480 nm period) were measured by detecting the PL signal with a spectrometer rotating with respect to the sample's normal at the angle of detection θ. More details on the experimental setup for PL measurements can be found in the Supporting Information (SI2, Figure S3(b)). The angular-wavelength maps of PL intensity are shown in Figures 4(a,b) for the PCs with d = 385 and d = 480 nm, respectively. Both maps possess maxima at 590, 597, 612, 618, and 625 nm associated with the emission of the Eu complex. The positions of these maxima are independent of the incident angle. However, the PL intensity has clear maxima along the spectral and angular positions of the SP excitation, as indicated by the white arrows. For the sample with a period of d = 385 nm, the PL intensity maxima are caused by the −1st SP, while for the second sample (d = 480 nm) the maxima result from the excitation of both +1st and −1st SP, which are symmetrically located around 0°. The angular dependence of the PL intensity at the electric dipole transition (λ = 612 nm) is shown in Figures 4(c,d), corresponding to Al PCs with a period of d = 385 and d = 480 nm, respectively. In the case of the first

https://doi.org/10.1021/acs.jpclett.5c02045
J. Phys. Chem. Lett. 2025, 16, 11590−11596

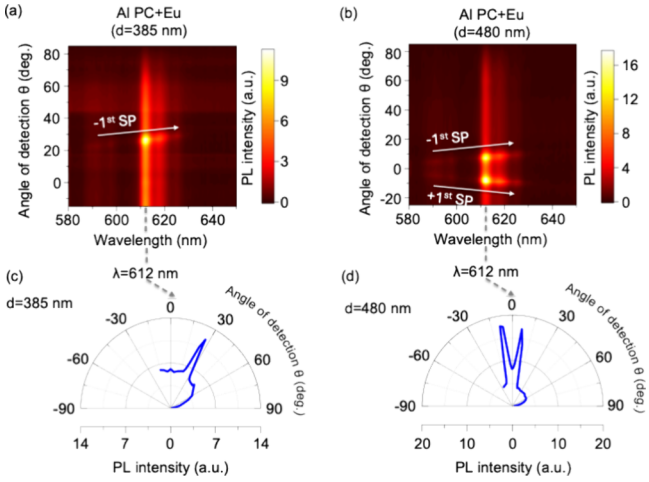

Figure 4. Angular dependences of the photoluminescence spectra of the Eu(dbm)$_3$(TDZP) films on the Al plasmonic crystals with a period of d = 385 nm (a) and d = 480 nm (b). The angular dependence of the PL intensity at the main emission line (λ = 612 nm) of the Eu(dbm)$_3$(TDZP) covered on the Al PCs with periods of d = 385 nm (c) and d = 480 nm (d).

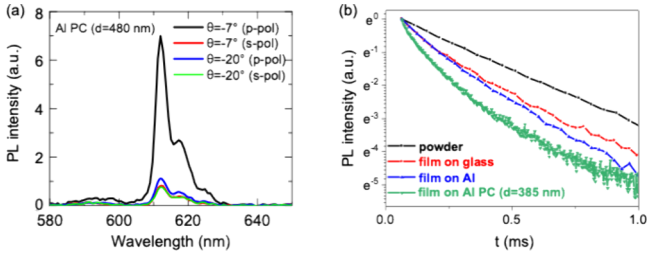

Figure 5. (a) Polarization-resolved photoluminescence spectra of the Eu complex deposited on Al PC (d = 480 nm). The spectra are taken at the resonant θ = −7° and nonresonant θ = −20° angles of detection. (b) Time decay curves of PL signal at λ = 612 nm for the Eu(dbm)$_3$(TDZP) complex in powder (black) and thin-film states upon the glass substrate (red), Al substrate (blue), and Al plasmonic crystal surfaces (green) with a period of d = 385 nm. The angle of detection is θ = 27°.

sample, the maximum is observed at θ = 27°. The second one has maxima at θ = ±7°, which are close to the surface normal of PCs. The PL intensities of both samples decrease when the detection angle does not correspond to SP excitation. As the detection angle increases, the intensity gradually decreases to zero as it approaches θ = 90°. The photoluminescence enhancement was calculated as the ratio of the maximum signal to the signal measured at the first nonresonant angle. For the first sample (d = 385 nm), the ratio is I(θ = 27°)/I(θ = 38°) = 2.3, and for the second sample (d = 480 nm) it is I(θ = 7°)/I(θ = 17°) = 4.1. The higher enhancement in the second sample is due to the higher Q-factor of its −1st SP. This is clearly visible in the narrow and dipper resonance in the reflectance spectrum of the second sample in Figures 3(c,d) (bottom graphs). The mechanism of the PL intensity enhancement is associated with an increase in the local density of the optical states (LDOS) due to SP resonances. The additional reason for this enhancement is an increase in extraction efficiency due to the outcoupling of SPs from PCs and their emission into the far-field, in accordance with the phase matching condition. The angular divergence $\Delta\theta$ of the PL emission was defined as full width at half-maximum (fwhm). For the first and second PCs $\Delta\theta$ is 5° and 6°, respectively.

The polarization analysis of the PL signal was performed by inserting a thin film polarizer after the filter in the experimental setup (Figure S3(b)). The polarizer's axis was aligned to allow the passing of either p-polarized light (parallel to the plane of light incidence) or s-polarized light (perpendicularly to the plane of incidence). The PL intensity spectra for the Al PC with a period of d = 480 nm are shown in Figure 5(a) at the resonant (θ = −7°) and nonresonant (θ = −20°) angles of detection. At the nonresonant angle (θ = −20°), both p- and s-polarized signals had similar intensities. However, at the resonant angle, the p-polarized signal was significantly stronger than the s-polarized one. This polarization selectivity can be attributed to the transverse magnetic origin of the SPs. Only the p-component of the emission can couple to SPs and re-emit radiation into the far field. Conversely, coupling with SPs is prohibited for s-polarized emission. Such a polarization difference at the resonant angle and almost identical intensity of both polarization components at nonresonant angles suggest that PL enhancement results from emission coupling with SPs.

The quantum yield (QY) measurements reveal significant differences for the europium-based complex deposited on different substrates, including quartz glass, aluminum, and aluminum PCs. All QY measurements were described in SI2. The QY on glass reaches 15 ± 5%. In contrast, the deposition on aluminum substrate reduces the QY down to 9 ± 5%. This decrease can be attributed to the enhanced nonradiative decay channels (Γ_{nonrad}) facilitated by a higher local density of optical states caused by the excitation of the SPs at the metal/Eu(dbm)$_3$(TDZP) interface. Specifically, the coupling between dipoles' emission and SPs in aluminum increases energy dissipation through nonradiative mechanisms, such as ohmic losses. Interestingly, the QY of the complex recovers back to 17 ± 5% when deposited on aluminum PCs. PC structures introduce a channel for the reemission of SPs to the far-field (increasing Γ_{rad}), which significantly suppresses unwanted absorption losses of plasmonic modes featured in a flat aluminum substrate.

To prove the impact of SPs on the Eu-based complex emission lifetime, time-correlated single-photon counting measurements were carried out. The results of the time-resolved photoluminescence signal recorded at λ = 612 nm and θ = 27° are shown in Figure 5(b) for 40 nm film of the Eu complex deposited on quartz glass (red curve), Al substrate (blue curve), and the PC with d = 385 nm (green curve). The PL signal from the powdered Eu complex (black curve) was collected via an integration sphere. More information about the fluorescence lifetime measurements can be found in the Supporting Information (SI3). By fitting the time-resolved photoluminescence intensity data (see fitting curves in SI 3, Figure S4) with $I(t) = I_1 e^{-t/\tau_{Eu}} + I_2 e^{-t/\tau_{sub}}$, the lifetime ($\tau_{Eu}$) of the Eu-based complex was determined (see derived τ_{Eu} and τ_{sub} values in Table S1, SI3). The τ_{sub} is the lifetime constant attributed to the small photoluminescence of the substrate on which Al was coated. The τ_{sub} is 0.05 ms and remains almost constant at all detection angles. The emission lifetime of the complex in the powder state is τ_{Eu} = 0.36 ms, which is consistent with other works.[58,59] The lifetime on the glass substrate is τ_{Eu}= 0.24 ms, indicating the intrinsic europium radiative decay rate. In the case of the aluminum substrate, the lifetime decreases down to τ_{Eu} = 0.20 ms, reflecting the

https://doi.org/10.1021/acs.jpclett.5c02045
J. Phys. Chem. Lett. 2025, 16, 11590−11596

enhanced nonradiative contributions (increasing the nonradiative decay rate, Γ_{nonrad}) due to surface plasmon excitation at the Al/air interface. This observation is in accordance with others experimental and theoretical works on the luminescence of the molecules located near metal surfaces.[60−62] The lifetime of the Eu-based complex deposited on the PC surface equals of τ_{Eu}= 0.14 ms, which is almost 1.5 times less than the lifetime of the emission from the nonstructured Al surface and 1.7 times less than the lifetime for the glass substrate. This lifetime reduction is associated with an additional radiative channel (increasing radiative decay rate, Γ_{rad}), which is connected to the outcoupling of the excited SPs with the following reradiation into the far-field. In the case of the SPs excitation on nonstructured Al surface, the phase matching forbids the reradiation of SPs to the far-field which leads to the ohmic damping of the PL signal. The latter explains the higher QY values in the case of PCs (17%) in comparison with a flat Al surface (9%). Figure S5 shows that, in the case of the Eu-based complex on the glass and Al substrate, the derived lifetimes are almost independent of the detection angle in the angle range from 15° to 70°. In the case of the PC, the minimum photoluminescence lifetime is observed at 27°, which matches the SP excitation angle at λ = 612 nm. The reduction in lifetime at specific angles aligns with the increased coupling of the PL emission to the SP modes and the enhanced outcoupling of photons into free space at resonant conditions. Additionally, we calculated the radiative lifetime (τ_{rad}) of the excited states of the Eu complex deposited on the PC with d = 385 nm at the resonant and nonresonant angles of detection (see details in SI4). The derived τ_{rad} equals 1.66 ms at the resonant angle of detection (θ=27°). The average τ_{rad} at nonresonant angles of detection (from θ = −15° to θ = 25° and from θ = 31° to θ = 41°) equals 2.67 ms, that is, 1.6 times higher than at the resonant angle. This clarifies the SP-induced origin of the observed PL enhancement.

These results underscore the dual role of plasmonic effects in modulating the luminescent properties. Although metallic surfaces can introduce detrimental quenching effects, carefully engineering a plasmonic crystal structure on the same substrate can counteract these losses and provide additional angular control over the emission. This finding highlights the potential of hybrid plasmonic architectures for designing tunable luminescent devices, particularly for applications that require high radiative efficiency and directional emission, such as narrow-band optical sources and luminescent sensors.

In conclusion, we have fabricated and optimized plasmonic surfaces for enhancing and controlling the photoluminescence of europium-based complexes. By tailoring plasmonic crystals, we achieved a strong directional emission with maxima at ±7°, which aligns with theoretical predictions. The 4-fold enhancement of the photoluminescence intensity near the main electric dipole emission line (λ = 612 nm) is observed due to the excitation of the SPs in plasmonic crystals in comparison with the nonresonance conditions. Under the SP resonant conditions, the photoluminescence lifetime decreases. The quantum yield measurements revealed a notable increase from 9% for the Eu-based complex on the nonstructured Al flat surface to 17% in the case of Al plasmonic crystals, with a 1.5-fold reduction in photoluminescence lifetime. These results highlight the potential of plasmonic crystal engineering to overcome waveguiding losses and improve the efficiency of lanthanide-based OLEDs, which are vital for advanced photonic applications in narrow-band directional emitters.

■ ASSOCIATED CONTENT

Supporting Information

The Supporting Information is available free of charge at https://pubs.acs.org/doi/10.1021/acs.jpclett.5c02045.

SI1, fabrication and characterization of the europium complex Eu(tta)$_3$(TDZP) (Figure S1) and atomic force microscopy map of the Eu(tta)$_3$(TDZP) film edge (Figure S2); SI2, the reflectance, photoluminescence, and quantum yield measurements (Figure 3(a,b)); SI3, photoluminescence lifetime measurements, fitting curves of photoluminescence time decay (Figure S4), and derived lifetime (Table S1) of Eu(tta)$_3$(TDZP) in the powder state and deposited on the Al flat film and Al plasmonic crystal at different detection angles (Figure S5); and SI4, calculation of the radiative lifetime of the excited states of the Eu complex deposited on the plasmonic crystals (Figure S6, Table S2) (PDF)

Transparent Peer Review report available (PDF)

■ AUTHOR INFORMATION

Corresponding Authors

Valentina V. Utochnikova − *Lomonosov Moscow State University, 119991 Moscow, Russia*; Email: valentina@utochnikova.ru

Andrey A. Fedyanin − *Lomonosov Moscow State University, 119991 Moscow, Russia*; orcid.org/0000-0003-4708-6895; Email: fedyanin@nanolab.phys.msu.ru

Authors

Aleksandr Yu. Frolov − *Lomonosov Moscow State University, 119991 Moscow, Russia; Shenzhen MSU-BIT University, 517182 Shenzhen, China*; orcid.org/0000-0003-0988-1361

Arseny Yu. Gladkikh − *Lomonosov Moscow State University, 119991 Moscow, Russia*

Matvey P. Belov − *Lomonosov Moscow State University, 119991 Moscow, Russia*

Vladimir V. Popov − *Lomonosov Moscow State University, 119991 Moscow, Russia*

Complete contact information is available at: https://pubs.acs.org/10.1021/acs.jpclett.5c02045

Author Contributions

M.P.B. and A.Y.F performed the luminescence and reflectance measurements; A.Y.F performed the AFM measurements; A.Y.G. and V.V.U. carried out the fabrication of the Eu complex and the lifetime photoluminescence measurements; V.V.P. fabricated the plasmonic crystals; all authors contributed to the writing of the manuscript; V.V.U. and A.A.F. supervised and conceptualized the project.

Notes

The authors declare no competing financial interest.

■ ACKNOWLEDGMENTS

This research was performed according to the Development Program of the Interdisciplinary Scientific and Educational School of Lomonosov Moscow State University "Photonic and Quantum Technologies. Digital Medicine." The study was conducted under the state assignment of Lomonosov Moscow State University. A.Yu. Frolov thanks the Russian Science Foundation (grant no. 24-72-00042) for supporting the experimental measurements in this work.

■ ABBREVIATIONS

dbm, dibenoylmethanate; TDZP, thiadiazolophenanthroline

■ REFERENCES

(1) Koden, M. *OLED Displays and Lighting* (Wiley/IEEE Press, 2017).
(2) Tsujimura, T. *OLED Display Fundamentals and Applications* (John Wiley & Sons Inc., 2017).
(3) Li, G.; Fleetham, T.; Turner, E.; Hang, X.-C.; Li, J. Highly Efficient and Stable Narrow-Band Phosphorescent Emitters for OLED Applications. *Adv. Opt Mater.* **2015**, *3* (3), 390−397.
(4) Utochnikova, V. V. Lanthanide complexes as OLED emitters. In *Handbook on the Physics and Chemistry of Rare Earths* (Elsevier B.V., 2021), pp 1−91.
(5) Bünzli, J. C. G. Rising Stars in Science and Technology: Luminescent Lanthanide Materials. *Eur. J. Inorg. Chem.* **2017**, *2017*, 5058−5063.
(6) Armelao, L.; Quici, S.; Barigelletti, F.; Accorsi, G.; Bottaro, G.; Cavazzini, M.; Tondello, E. Design of luminescent lanthanide complexes: From molecules to highly efficient photo-emitting materials. *Coord. Chem. Rev.* **2010**, *254* (5), 487−505.
(7) Utochnikova, V. V.; Aslandukov, A. N.; Vashchenko, A. A.; Goloveshkin, A. S.; Alexandrov, A. A.; Grzibovskis, R.; Bünzli, J. C. G. Identifying lifetime as one of the key parameters responsible for the low brightness of lanthanide-based OLEDs. *Dalton Transactions* **2021**, *50* (37), 12806−12813.
(8) Wang, Q.; Lin, S.; Ming, C.; Zhao, H.; Liu, J.; Zhang, C.; Song, F.; Pun, E. Y. B. Plasmon-enhanced luminescence of Eu complex by using silver nanocubes for different excitations. *Mater. Lett.* **2011**, *65* (5), 905−907.
(9) Liu, F.; Aldea, G.; Nunzi, J. M. Metal plasmon enhanced europium complex luminescence. *J. Lumin.* **2010**, *130* (1), 56−59.
(10) Zhang, J.; Cheng, X.; Zhang, H.; Zheng, J.; Wang, J. Plasmon-Controlled Selective Emission Enhancement of Eu3+with (Au Core)@(Y(V,P)O4:Eu) Nanostructures. *ACS Nano* **2023**, *17* (11), 10546−10559.
(11) Lozano, G.; Rodriguez, S. R. K.; Verschuuren, M. A.; Rivas, J. G. Metallic nanostructures for efficient LED lighting. *Light Sci. Appl.* **2016**, *5* (6), e16080−e16080.
(12) Hancu, I. M.; Curto, A. G.; Castro-López, M.; Kuttge, M.; Van Hulst, N. F. Multipolar interference for directed light emission. *Nano Lett.* **2014**, *14* (1), 166−171.
(13) Kinkhabwala, A.; Yu, Z.; Fan, S.; Avlasevich, Y.; Müllen, K.; Moerner, W. E. Large single-molecule fluorescence enhancements produced by a bowtie nanoantenna. *Nat. Photonics* **2009**, *3* (11), 654−657.
(14) Wang, M.; Hu, C.; Su, Q. Luminescent Lifetime Regulation of Lanthanide-Doped Nanoparticles for Biosensing. *Biosensors (Basel)* **2022**, *12* (2), 131.
(15) Gladkikh, A. Y.; Kozlov, M. I.; Vashchenko, A. A.; Medved'ko, A. V.; Goloveshkin, A. S.; Bolshakova, A. V.; Latipov, E. V.; Utochnikova, V. V. A 50% increase in the terbium-based OLED luminance through reducing the excited-state lifetime due to the introduction of gold nanoparticles. *Dalton Transactions* **2022**, *51* (42), 16065−16069.
(16) Regmi, R.; Berthelot, J.; Winkler, P. M.; Mivelle, M.; Proust, J.; Bedu, F.; Ozerov, I.; Begou, T.; Lumeau, J.; Rigneault, H.; García-Parajó, M. F.; Bidault, S.; Wenger, J.; Bonod, N. All-Dielectric Silicon Nanogap Antennas to Enhance the Fluorescence of Single Molecules. *Nano Lett.* **2016**, *16* (8), 5143−5151.
(17) Zyuzin, M. V.; Baranov, D. G.; Escudero, A.; Chakraborty, I.; Tsypkin, A.; Ushakova, E. V.; Kraus, F.; Parak, W. J.; Makarov, S. V. Photoluminescence quenching of dye molecules near a resonant silicon nanoparticle. *Sci. Rep* **2018**, *8* (1), 6107.
(18) Vidal, C.; Tilmann, B.; Tiwari, S.; Raziman, T. V.; Maier, S. A.; Wenger, J.; Sapienza, R. Fluorescence Enhancement in Topologically Optimized Gallium Phosphide All-Dielectric Nanoantennas. *Nano Lett.* **2024**, *24* (8), 2437−2443.
(19) Baranov, D. G.; Savelev, R. S.; Li, S. V.; Krasnok, A. E.; Alù, A. Modifying magnetic dipole spontaneous emission with nanophotonic structures. *Laser Photon Rev.* **2017**, *11* (3), 1600268.
(20) Rutckaia, V.; Heyroth, F.; Novikov, A.; Shaleev, M.; Petrov, M.; Schilling, J. Quantum Dot Emission Driven by Mie Resonances in Silicon Nanostructures. *Nano Lett.* **2017**, *17* (11), 6886−6892.
(21) Soboleva, I. V.; Descrovi, E.; Summonte, C.; Fedyanin, A. A.; Giorgis, F. Fluorescence emission enhanced by surface electromagnetic waves on one-dimensional photonic crystals. *Appl. Phys. Lett.* **2009**, *94* (23), 231122.
(22) Genevet, P.; Capasso, F.; Aieta, F.; Khorasaninejad, M.; Devlin, R. Recent advances in planar optics: from plasmonic to dielectric metasurfaces. *Optica* **2017**, *4* (1), 139.
(23) Hussain, R.; Kruk, S. S.; Bonner, C. E.; Noginov, M. A.; Staude, I.; Kivshar, Y. S.; Noginova, N.; Neshev, D. N. Enhancing Eû3+ magnetic dipole emission by resonant plasmonic nanostructures. *Opt. Lett.* **2015**, *40* (8), 1659.
(24) Lozano, G.; Grzela, G.; Verschuuren, M. A.; Ramezani, M.; Rivas, J. G. Tailor-made directional emission in nanoimprinted plasmonic-based light-emitting devices. *Nanoscale* **2014**, *6* (15), 9223−9229.
(25) Sergeeva, K. A.; Pavlov, D. V.; Seredin, A. A.; Mitsai, E. V.; Sergeev, A. A.; Modin, E. B.; Sokolova, A. V.; Lau, T. C.; Baryshnikova, K. V.; Petrov, M. I.; Kershaw, S. V.; Kuchmizhak, A. A.; Wong, K. S.; Rogach, A. L. Laser-Printed Plasmonic Metasurface Supporting Bound States in the Continuum Enhances and Shapes Infrared Spontaneous Emission of Coupled HgTe Quantum Dots. *Adv. Funct Mater.* **2023**, *33* (44), 2307660.
(26) Piccotti, D.; Trevisani, M.; Pirruccio, G.; Kalinic, B.; Cesca, T.; Mattei, G. Polarized coherent emission outside high-symmetry points of dye-coupled plasmonic lattices. *Phys. Chem. Chem. Phys.* **2023**, *25* (12), 8641−8650.
(27) Giannini, V.; Vecchi, G.; Gómez Rivas, J. Lighting up multipolar surface plasmon polaritons by collective resonances in arrays of nanoantennas. *Phys. Rev. Lett.* **2010**, *105* (26), 266801.
(28) Zakharko, Y.; Graf, A.; Zaumseil, J. Plasmonic Crystals for Strong Light-Matter Coupling in Carbon Nanotubes. *Nano Lett.* **2016**, *16* (10), 6504−6510.
(29) Dyakov, S. A.; Zhigunov, D. M.; Marinins, A.; Shalygina, O. A.; Vabishchevich, P. P.; Shcherbakov, M. R.; Presnov, D. E.; Fedyanin, A. A.; Kashkarov, P. K.; Popov, S.; Gippius, N. A.; Tikhodeev, S. G. Plasmon induced modification of silicon nanocrystals photoluminescence in presence of gold nanostripes. *Sci. Rep* **2018**, *8* (1), 4911.
(30) Kalinic, B.; Cesca, T.; Mignuzzi, S.; Jacassi, A.; Balasa, I. G.; Maier, S. A.; Sapienza, R.; Mattei, G. All-Dielectric Silicon Nanoslots for Er3+ Photoluminescence Enhancement. *Phys. Rev. Appl.* **2020**, *14* (1), 014086.
(31) Liu, S.; Vaskin, A.; Addamane, S.; Leung, B.; Tsai, M. C.; Yang, Y.; Vabishchevich, P. P.; Keeler, G. A.; Wang, G.; He, X.; Kim, Y.; Hartmann, N. F.; Htoon, H.; Doorn, S. K.; Zilk, M.; Pertsch, T.; Balakrishnan, G.; Sinclair, M. B.; Staude, I.; Brener, I. Light-Emitting Metasurfaces: Simultaneous Control of Spontaneous Emission and Far-Field Radiation. *Nano Lett.* **2018**, *18* (11), 6906−6914.
(32) Vaskin, A.; Bohn, J.; Chong, K. E.; Bucher, T.; Zilk, M.; Choi, D. Y.; Neshev, D. N.; Kivshar, Y. S.; Pertsch, T.; Staude, I. Directional and Spectral Shaping of Light Emission with Mie-Resonant Silicon Nanoantenna Arrays. *ACS Photonics* **2018**, *5* (4), 1359−1364.
(33) Kroychuk, M. K.; Shorokhov, A. S.; Yagudin, D. F.; Rakhlin, M. V.; Klimko, G. V.; Toropov, A. A.; Shubina, T. V.; Fedyanin, A. A. Quantum Dot Photoluminescence Enhancement in GaAs Nanopillar Oligomers Driven by Collective Magnetic Modes. *Nanomaterials* **2023**, *13* (3), 507.
(34) Xiong, Y.; Huang, Q.; Canady, T. D.; Barya, P.; Liu, S.; Arogundade, O. H.; Race, C. M.; Che, C.; Wang, X.; Zhou, L.; Wang, X.; Kohli, M.; Smith, A. M.; Cunningham, B. T. Photonic crystal enhanced fluorescence emission and blinking suppression for single quantum dot digital resolution biosensing. *Nat. Commun.* **2022**, *13* (1), 4647.

https://doi.org/10.1021/acs.jpclett.5c02045
J. Phys. Chem. Lett. 2025, 16, 11590−11596

(35) Vaskin, A.; Mashhadi, S.; Steinert, M.; Chong, K. E.; Keene, D.; Nanz, S.; Abass, A.; Rusak, E.; Choi, D. Y.; Fernandez-Corbaton, I.; Pertsch, T.; Rockstuhl, C.; Noginov, M. A.; Kivshar, Y. S.; Neshev, D. N.; Noginova, N.; Staude, I. Manipulation of Magnetic Dipole Emission from Eu 3+ with Mie-Resonant Dielectric Metasurfaces. *Nano Lett.* **2019**, *19* (2), 1015−1022.
(36) Sugimoto, H.; Fujii, M. Magnetic Purcell Enhancement by Magnetic Quadrupole Resonance of Dielectric Nanosphere Antenna. *ACS Photonics* **2021**, *8* (6), 1794−1800.
(37) Bashiri, A.; Vaskin, A.; Tanaka, K.; Steinert, M.; Pertsch, T.; Staude, I. Color Routing of the Emission from Magnetic and Electric Dipole Transitions of Eu3+ by Broken-Symmetry TiO2Metasurfaces. *ACS Nano* **2024**, *18* (1), 506−514.
(38) Chen, X.; Sun, T.; Wang, F. Lanthanide-Based Luminescent Materials for Waveguide and Lasing. *Chem. Asian J.* **2020**, *15* (1), 21−33.
(39) Fernandez-Bravo, A.; Wang, D.; Barnard, E. S.; Teitelboim, A.; Tajon, C.; Guan, J.; Schatz, G. C.; Cohen, B. E.; Chan, E. M.; Schuck, P. J.; Odom, T. W. Ultralow-threshold, continuous-wave upconverting lasing from subwavelength plasmons. *Nat. Mater.* **2019**, *18* (11), 1172−1176.
(40) Guo, L.; Ji, M.; Kang, B.; Zhang, M.; Xie, X.; Wu, Z.; Chen, H.; Deckert, V.; Zhang, Z. Plasmon-assisted mode selection lasing in a lanthanide-based microcavity. *Advanced Photonics* **2024**, *6* (3), 035001.
(41) Dabard, C.; Bossavit, E.; Dang, T. H.; Ledos, N.; Cavallo, M.; Khalili, A.; Zhang, H.; Alchaar, R.; Patriarche, G.; Vasanelli, A.; et al. Electroluminescence and Plasmon-Assisted Directional Photoluminescence from 2D HgTe Nanoplatelets. *J. Phys. Chem. C* **2023**, *127* (30), 14847−14855.
(42) Lupton, J. M.; Matterson, B. J.; Samuel, I. D. W.; Jory, M. J.; Barnes, W. L. Bragg scattering from periodically microstructured light emitting diodes. *Appl. Phys. Lett.* **2000**, *77* (21), 3340−3342.
(43) Huang, K. C. Y.; Seo, M. K.; Huo, Y.; Sarmiento, T.; Harris, J. S.; Brongersma, M. L. Antenna electrodes for controlling electroluminescence. *Nat. Commun.* **2012**, *3* (1), 1005.
(44) Hobson, P. A.; Wedge, S.; Wasey, J. A. E.; Sage, I.; Barnes, W. L. Surface Plasmon Mediated Emission from Organic Light-Emitting Diodes. *Adv. Mater.* **2002**, *14* (19), 1393−1396.
(45) Yang, A.; Li, Z.; Knudson, M. P.; Hryn, A. J.; Wang, W.; Aydin, K.; Odom, T. W. Unidirectional Lasing from Template-Stripped Two-Dimensional Plasmonic Crystals. *ACS Nano* **2015**, *9* (12), 11582−11588.
(46) Barnes, W. L.; Preist, T. W.; Kitson, S. C.; Sambles, J. R. Physical origin of photonic energy gaps in the propagation of surface plasmons on gratings. *Phys. Rev. B* **1996**, *54* (9), 6227.
(47) Hakala, T. K.; Rekola, H. T.; Väkeväinen, A. I.; Martikainen, J. P.; Nečada, M.; Moilanen, A. J.; Törmä, P. Lasing in dark and bright modes of a finite-sized plasmonic lattice. *Nat. Commun.* **2017**, *8* (1), 13687.
(48) Bossavit, E.; Dang, T. H.; He, P.; Cavallo, M.; Khalili, A.; Dabard, C.; Zhang, H.; Gacemi, D.; Silly, M. G.; Abadie, C.; Gallas, B.; Pierucci, D.; Todorov, Y.; Sirtori, C.; Diroll, B. T.; Degiron, A.; Lhuillier, E.; Vasanelli, A. Plasmon-Assisted Directional Infrared Photoluminescence of HgTe Nanocrystals. *Adv. Opt Mater.* **2023**, *11* (22), 2300863.
(49) Mashhadi, S.; Durach, M.; Keene, D.; Noginova, N. Control of magnetic dipole emission with surface plasmon polaritons. *OSA Contin* **2019**, *2* (4), 1342.
(50) Knight, M. W.; King, N. S.; Liu, L.; Everitt, H. O.; Nordlander, P.; Halas, N. J. Aluminum for plasmonics. *ACS Nano* **2014**, *8* (1), 834−840.
(51) Geffroy, B.; le Roy, P.; Prat, C. Organic light-emitting diode (OLED) technology: Materials, devices and display technologies. *Polym. Int.* **2006**, *55* (6), 572−582.
(52) Bauri, J.; Choudhary, R. B.; Mandal, G. Recent advances in efficient emissive materials-based OLED applications: a review. *J. Mater. Sci.* **2021**, *56* (34), 18837−18866.
(53) Kornikov, A. I.; Kozlov, M. I.; Vashchenko, A. A.; Pavlov, A. A.; Gordeeva, E. O.; Latipov, E. V.; Lepnev, L. S.; Kozhevnikova, V. Y.; Utochnikova, V. V. First Dual Red-Near-Infrared Emissive Solution-Processed Organic Light-Emitting Diode Based on Europium-Ytterbium Mixed-Ligand Complexes for Pulse Oximetry. *ACS Applied Optical Materials* **2023**, *1* (7), 1227−1235.
(54) Raether, H. *Surface Plasmons on Smooth and Rough Surfaces and on Gratings* (Springer-Verlag, 1988).
(55) Kiryanov, M. A.; Frolov, A.Yu.; Novikov, I. A.; Kipp, P. A.; Nurgalieva, P. K.; Popov, V. V.; Ezhov, A. A.; Dolgova, T. V.; Fedyanin, A. A. Surface profile-tailored magneto-optics in magneto-plasmonic crystals. *APL Photonics* **2022**, *7* (2), 026104.
(56) Watts, R. A.; Hibbins, A. P.; Sambles, J. R. The infuence of grating profile on surface plasmon polariton resonances recorded in different diffracted orders. *J. Mod. Opt* **1999**, *46* (15), 2157−2186.
(57) Makarova, A. V.; Nerovnaya, A. A.; Gulkin, D. N.; Popov, V. V.; Frolov, A. Y.; Fedyanin, A. A. Goos-Hänchen Shift Spatially Resolves Magneto-Optical Kerr Effect Enhancement in Magnetoplasmonic Crystals. *ACS Photonics* **2024**, *11* (4), 1619−1626.
(58) Sun, P. P.; Duan, J. P.; Lih, J. J.; Cheng, C. H. Synthesis of New Europium Complexes and Their Application in Electroluminescent Devices. *Adv. Funct Mater.* **2003**, *13* (9), 683−691.
(59) Gallardo, H.; Conte, G.; Tuzimoto, P.; Bortoluzzi, A.; Peralta, R. A.; Neves, A. Synthesis, crystal structure and luminescent properties of new tris-β-diketonate Eu(III) complex with thiadiazolophenanthroline derivative ligand. *Inorg. Chem. Commun.* **2008**, *11* (10), 1292−1296.
(60) Chance, R. R.; Miller, A. H.; Prock, A.; Silbey, R. Fluorescence and energy transfer near interfaces: The complete and quantitative description of the Eu+3/mirror systems. *J. Chem. Phys.* **1975**, *63* (4), 1589−1595.
(61) Chance, R. R.; Prock, A.; Silbey, R. *Molecular Fluorescence and Energy Transfer Near Interfaces*; (1978), pp 1−65.
(62) Morawitz, H.; Philpott, M. R. Coupling of an excited molecule to surface plasmons. *Phys. Rev. B* **1974**, *10* (12), 4863−4868.

https://doi.org/10.1021/acs.jpclett.5c02045
J. Phys. Chem. Lett. 2025, 16, 11590−11596